Chemistry and Materials Research
ISSN 2224- 3224 (Print) ISSN 2225- 0956 (Online)
Vol.14 No.4, 2022

Microstructural transformations and Grain growth in alumina nanoprecursors

Fadia Shaheen (Corresponding author)
Glass and Ceramic Research Centre, PCSIR Laboratories Complex, Lahore, Pakistan
Tel: +92 042 99230688-95 E-mail: Fadia.shaheen@hotmail.com

Khalid Javed
Glass and Ceramic Research Centre, PCSIR Laboratories Complex, Lahore, Pakistan
Tel: +92 042 99230688-95 E-mail: khalidpcsir@gmail.com

Tayyaba Ahmad
Applied Chemistry Research Centre, Lahore, Pakistan
Tel: +92 042 99230688-95 E-mail: tayyabah@hotmail.com

Muhammad Latif Mirza
Department of Chemistry, University of Sargodha, Sargodha, Pakistan
Tel: +92 048- 111-867-111 E-mail: mlatifmirza@yahoo.com

Abstract:
Alumina nanoprecursors with a range of average particle size and narrow distribution manifested two different grain and pore growth during mictrostructural developments. Densification temperature decreases in general with the decrease in average particle size though the distribution of particle size as a function of heating rate manifested different grain growth and subsequent densification. At low heating rate, 5°C the particles tend to show bimodal grain growth with bigger average grain, about 3 micron and densified at elevated temperatures, 1600°C. While at ten times elevated heating rate, 50°C, the particles tend to show normal grain growth with desirable average grain, 1bout 1 micron and densified at comparatively 200°C degrees lower temperature.
Keywords:Alumina, densification, grain growth, pore closure.
DOI: 10.7176/CMR/14-4-04
Publication date: November 30th, 2022

Introductions:
Research in the densification and microscopic studies of alumina Al_2O_3 owe to its versatile structural and functional properties such as high thermal conductivity, high hardness, and a good resistance to corrosion and abrasion (Kasprzyk-Hordern. 2004) It finds applications in the aerospace (Rathod 2017), filtration and cooling systems, water treatment (Bhatnagar *et al* 2010, Sarkar *et al* 2012 and Sridhara *et al* 2011), medical fields (Sadiq *et al* 2009, Becker *et al* 2016 and Mahmoudian *et al* 2019), engineering materials (Chevalier *et al* 2009, Hulbert *et al* 1993 and Benzaid *et al* 2008). Alumina as coating on aluminium improves wear resistance (Valant *et al* 2016) and also serve as electrical and thermal insulation (He *et al* 2009).

Generally most properties are enhanced by smaller grain size, a notable exception being the creep resistance which increases with larger grain size. A wide range of electrical and magnetic phenomena are affected by grain size, and it is in this area that grain size control has been used most effectively to produce ceramics with properties suitable for a variety of applications.

Ceramics firing demands elevated energy as it accounts for ≅ 83% of the energy consumed for their production (Brinkerhoff *et al* 2015). Now a days modern ceramic processing are being evolved to reduce the firing temperature as well as firing span keeping in view environmental and economic issues. Study of grain growth is an area of interest for fields of improved mechanical properties (Kermani *et al* 2021 and Dong *et al* 2021) and optical properties. (Krell *et al* 2003 and Apetz 2003)

Fast firing is a method to lower down the densification time. In particular, in the case of alumina it can also inhibit grain growth as the activation energy of densification is higher than that of coarsening (Harmer *et al* 1981 and Rahaman *et al* 2017). In recent years, various densification methods have been evolved. Fast Firing (FF) Harmer *et al* 1981), Microwave Sintering (MWS) (Katz et al 1992), Spark Plasma Sintering (SPS) (Grasso *et al* 2009), Flash Sintering (FS) (Cologna *et al* 2010), and Ultra-fast High-temperature Sintering

(UHS) (Wang *et al* 2020) have pushed heating rate limits up to 102 –104 ◦C/min (Biesuz *et al* 2019, Biesuz *et al* 2020 and Yu *et al* 2017).

Experimental:

Nanoprecursors with four different average particle size as shown in Figure 1 were used for sintering studies. The compositions named A1, A2, A3 and A4 were consolidated into green bodies. After presintering at 800ºC for 2 hours, the powders were damped with 2wt% (related to Al_2O_3) polyvinyl alcohol PVA (Hoechst, Frankfurt) and uniaxially pressed into 1X0.3" disks. The prerequisites and parameters of cold compaction are given in Table 1.

The green machined compacts were initially dried overnight at room temperature, heated at 100ºC for 1 hour in electric oven and finally thermolysed at 800ºC for 1 hour. The digital electric laboratory oven WE 500HA and high temperature rapid heating electric furnace RHF/3 Carbolite, UK were used. Sintering was carried out by employing two heating programmes, In heating programme-I, as sketched in Figure 2, a specimen was fired at five different temperatures i.e. 1000, 1100, 1200, 1300, 1400, 1500, and 1600ºC.

In the first step, specimen was fired at 1000ºC at the rate of 5ºC per minute. The temperature was maintained for 3 hours and furnace was switched off. Once it cooled down to room temperature, the specimen was collected for SEM studies and so on so far. While in programme-II, specimen were fired @ 50ºC per minute and soaked at 1400ºC for 3 hours. For TDA, specimens with 50 mm length and 20 mm width were fired up to 1600oC @ 20ºC per minute in Horizontal Orton Dilatometer DIL 2016 STD. A Hitachi S-3700, Japan SEM equipped with EDS, was used to acquire image at the accelerating voltage 25 kV, working distance 5 mm, tilt angle 0º.

Result and Discussion

The particle size distribution is graphically presented with the respective micrograph in Figure 3. SEM image reveals have narrow particle size distribution. The particles were round and well dispersed. The compaction results of green bodies were examined by topological and transparency analyses. Composition A1 after die compaction is shown in Figure -a. The surface of the disk appears flawless. There could not be seen cracks. It was also found translucent indicating that pores are smaller than the visible light wavelength which is most desirable for high density densification.

a. SEM Microstructural studies during heating programme-I

Following heating programme-I, compositions were fired at 1000ºC. The microstructure of sA1 is presented in Figure 4. After firing at 1000ºC, the Figure 4a shows that the pores in the structure ensure complete burn out of the binder. Moreover, their even distribution shows that polyvinyl alcohol was thoroughly mixed with the powder.

On firing sample at 1100ºC, some change in the surface can be noticed. In Figure 4b smoothing of surface revels that the sample has started responding to heat. The pore distribution has become little bit more clear. At certain points they seem interconnected to each other in winding course. A larger number of initial point contacts can be seen.

The sample after firing at 1200ºC is shown in Figure 4c. It seems that the particles started joining to form the necks. The interconnected pores also seem rounding off.

The surface smoothing of the particles became obvious on firing at 1300ºC as shown in Figure 4d. Figure 4e shows sample fired at 1400ºC temperature. The grain growth in the SEM image shows that the sintering has reached the intermediate stage. The grains have defined their boundaries. Considerable growth at the grain boundaries can be seen. The shrinkage of pores is also in progress. Augmentation in structure which appeared in the initial stages of sintering is also becoming obvious.

Firing at 1500ºC brought about a substantial increase in grain growth as obvious in Figure 4f. The sample also showed a significant decrease in mean porosity. The interconnected pores seem pinched into isolated pores, collectively representing the beginning of the final stage.

The sintering of sample seems completed on firing at 1600ºC as the sample in Figure 4g shows complete closure of pores.

The SEM images of microstructural developments during sintering of A2, A3 and A4 compositions are presented in Figure 5. The dilatometric curve as depicted in Figure 6 shows that up to 800ºC, the sample shows linear shrinkage in three steps with the corresponding peaks of shrinkage rate. First percent linear change of 0.16% relates to the evolution of adsorbed water, second 0.58% to the dehydroxylation of pseudoboehmite, and third 1.22% to transformation into gamma alumina with the consequent peaks of shrinkage rate at 100, 231 and 325ºC, respectively.

The linear shrinkage from 800 to 1400ºC is 2.14% which depicts sintering behavior of sample. It can be seen in Figure that densification began at 895ºC. Of 2.14%, almost 80% shrinkage completed up to 1100ºC and the remaining 20% up to 1300ºC at comparatively slow pace.

There are two broad peaks associated with the percentage linear shrinkage curve from 800 to 1400ºC. The peak with minimum shrinkage rate named T_1 appeared at 1020ºC and with maximum shrinkage rate T_2 at 1098ºC. The general appearance of dilatometric curves of three specimens is same. However, linear shrinkage curves onset at 895, 899, 905, and 911ºC, respectively. T_1 and T_2 peaks are ultimately shifted to higher temperatures by few degrees. First peak appeared at 1020, 1024, 1030 and 1036 and second at 1098, 1102, 1109, and 1116ºC, respectively. Dilatometric analysis concludes that sinterability of alumina nanoprecursors decreases with increase in average particle size.

b. SEM microstructural studies during heating programme-II

A1 composition was fired at 1000 and 1400ºC following heating programme-II. Sample A1 was fired at 1000ºC is presented in Figure 7a. The image witnesses surface smoothing of sample with neck growth to high extent. The sample seems entering into intermediate stage with certain pores interconnected while higher population has rounded off.

Sample on firing at 1400ºC is shown in Figure 7b. The micrograph ascertains that sintering is completed. The pores are closed intersecting at the grain boundaries. There is no coarsening or augmentation in structure. The grain size is isotropic with almost equiaxial grain shapes. The sintering results show compliance with the dilatometric results.

The SEM images of A2, A3, and A4 compositions sintering at 1400ºC following heating programme-II are shown in Figure 8. Alumina sintered bodies show an average grain size nearly 1micron which is quite desirable.

Abnormal grain growth during heating programme-I

The grain growth during heating according to programme-I seems bimodal. There are two kinds of grains, either too big or too small. The two categories of grains have uniform grain growth. The bigger grains have an average size of about 3 and smaller ones of about 0.3 microns. If seen categorically, growth is a combination of normal and abnormal. Normal growth occurs in one category which is abnormal with reference to other category. The course of grain growth is presented in Figure 9a. The sequential change in microstructure develops an understanding that particles join to make ring like structures of an average size 3 microns while those left in between are constrained and their growth is restricted to too small grains with an average size 0.3 micron. Figure b and c were acquired at tilted position to have a better orientation of grain growth.

Figure 9d highlights the growth of an exaggerated grain. Atoms in the grain boundary have higher energy than in the bulk of the crystalline grain therefore these join to make a ring like boundary. The width of grain boundary is about 1.2 microns. The pores inside the large abnormal grain are of two kinds. The bigger pores with irregular shape and average size up to 1 micron occupy the peripheral position in the grain whereas the smaller pores with circular shape and average size down to 0.2 micron are central. The augmentation of structure at certain points gives fallacy impression of pores. It was observed that on heating the smaller pores eliminate earlier due to short diffusion distance for matter transport from the pore boundary whereas larger pores take longer time to eliminate due to long diffusion distance.

The grains at the boundary of this exaggerated grain followed the same pattern of pore elimination. The micrograph reveals that when the pore elimination in bigger grain is far away from completion, the elimination is completed in too small grains on its boundary.

Normal grain growth during heating programme-II

On sintering nanopowders in accordance with the programme-II, grain growth is isotropic. The frame work of grains is presented in Figure 10a. It can be seen that the average size and shape of grain is relative to grain on following heating schedule-I is narrower ranged. A fine array of pores network shows that most of the pores are spherical in shape with average size 100nm or even less therefore are far more easier to remove during sintering because of short diffusion distances in comparison to those encountered during abnormal grain growth. Figure 10b elaborates interconnected pores pinching off and shrinkage of isolated pores. The pockets on the surface of the grain are in fact the vestiges of pores and absolutely do not interfere in the density measurements as these are perfectly closed.

Conclusion

The control of grain growth during sintering is one of the most important considerations in the fabrication of ceramics for two key reasons. First, many engineering properties of ceramics are dependent on the grain size, so grain growth control is directly related to the achievement of the desired properties. Second, grain growth increases the diffusion distance for matter transport, thereby reducing the rate of densification, and therefore is plays key role to achieve high density.

The particle size distribution of alumina nanoprecursors relevance to heating and cooling rates affected the grain growth differently. At lower heating rate the particles showed bimodal grain growth with exaggerated coarsened grain and closure of bigger pores at elevated temperatures. While at higher heating rate the particles showed isotropic grain with closure of pores at relatively lower temperatures.

References

Apetz. R., Bruggen. M. P. B. V (2003) “Transparent alumina: a light-scattering model” Journal American Ceramic Society **86**, 480–486,

Becker, L. C. Boyer, I. Bergfeld, W. F. Belsito, D. V., Hill, R. A. Klaassen, C. D. Liebler, D. C. Marks, J. G., Shank, J. R. C., Slaga, T. J et al. (2016) “Safety assessment of alumina and aluminum hydroxide as used in cosmetics”. International Journal of Toxicology, **35**(3 suppl), 16S–33S.

Benzaid, R., Chevalier, J., Saˆadaoui, M., Fantozzi G., Nawa. M., Diaz. L. A. and Torrecillas. R (2008) “Fracture toughness, strength and slow crack growth in a ceria stabilized zirconia–alumina nanocomposite for medical applications”. Biomaterials, **29** (27), 3636–3641.

Biesuz. M., Grasso. S., Sglavo. M. (2020) “What’s new in ceramics sintering A short report on the latest trends and furture propects.” Solid State Materials Sciences **24** 100868.

Biesuz. M., Sglavo. V. M., (2019) “Flash sintering of ceramics,” Journal Europeon Ceramic Society. **39,**115-143.

Bhatnagar, A., Kumar, E. and Sillanp¨a¨a, M. (2010) “Nitrate removal from water by nanoalumina: Characterization and sorption studies.” Chemical Engineering Journal, **163**(3), 317–323.

Brinkerhoff. WSP. B.,, GL. DNV (2015) Industrial Decarbonisation & Energy Efficiency Roadmaps to 2050, Ceramic sector.

Chevalier, J and Gremillard. L. (2009) “Ceramics for medical applications: A picture for the next 20 years”. Journal of the European Ceramic Society, **29**(7), 1245–1255.

Cologna. M., Rashkova. B., Raj. R (2010) “Flash Sintering of Nanograin Zirconia in <5 s at 850°C” Journal American Ceramic Society **93**, 3556-9

Dong. J., Pouchly. V., Biesuz. M., Tyrpekl. V., Vil´emova. M., Kermani., Reece. M., Hu. C., Grasso. S (2021) “Thermally-insulated ultra-fast high temperature sintering (UHS) of zirconia: a master sintering curve analysis,” Scripta Mater. **203,** 114076,

Grasso. S., Sakka.Y., Maizza. G. (2009) “Electric current activated/assisted sintering (ECAS) a review of patents” Science Technology Advanced Materials. **10**, 1906-2008.

Harmer. M. P., Brook. R. J. (1981) “Fast firing - microstructural benefits”, Transaction Journal British Ceramic Society **80**, 147–148.

He. O., Zheng. D. and Hu.S (2009) “Development and application of a nanoalumina based nitric oxide sensor”. Microchimica Acta, **164**(3-4), 459–464.

Hulbert. SF (1993) “The use of alumina and zirconia in surgical implants”. Advanced Series in Ceramics, **1**, 25–40.

Kasprzyk-Hordern. B. (2004) “Chemistry of alumina, reactions in aqueous solution and its application in water treatment”. Advances in Colloid and Interface Science **110**(1-2), 19–48.

Mahmoudian, M. Marjani, A. P, Hasanzadeh, R., Nozad, E., Shishavan, E. M and Mohamadi. H (2019) "Effect of in-situ modification of α-alumina nanoparticles on mechanical properties of poly (methyl methacrylate)-based 24 nanocomposites for biomedical applications." Materials Research Express, **6**(10), 105410.

Rahaman. M. N (2017) Ceramic Processing and Sintering, second ed., 2end ed.

Rathod, S. T., Kumar, J. S., and Jain, A. (2017) "Polymer and ceramic nanocomposites for aerospace applications". Applied Nanoscience, **7**(8), 519–548,

Sadiq, I. M., Chowdhury, B., Chandrasekaran, N. and Mukherjee. A. (2009) "Antimicrobial sensitivity of escherichia coli to alumina nanoparticles." Nanomedicine: Nanotechnology, Biology and Medicine, **5**(3), 282–286.

Sarkar, S., Bandyopadhyay, S., Larbot, A. and Cerneaux. S. (2012) "New clay–alumina porous capillary supports for filtration application". Journal of Membrane Science, **392**,130–136.

Sridhara, V and Satapathy, L. N. (2011) "Al_2O_3-based nanofluids: a review". Nanoscale Research Letters, **6**(1), 456.

Valant. M., Luin. U., Fanetti,M., Mavri˘c.A., Vyshniakova.K., Siketi´c. Z.,, and Kalin. M., (2016) "Fully transparent nanocomposite coating with an amorphous alumina matrix and exceptional wear and scratch resistance." Advanced Functional Materials, **26**(24), 4362–4369.

Katz. D. (1992) Microwave sintering of ceramics, Annual Review Material Sciences. **22**, 153–170.

Kermani. M., Dong. J., Biesuz. M., Linx. Y., Deng. H., Sglavo. V. M., Reec. M. J., Hu. C., Grasso. S., (2021) "Ultrafast high-temperature sintering (UHS) of fine grained α-Al2O3." Journal European Ceramic Society. **41**, 6626–6633.

Krell. A., Blank. P., Ma. H, Hutzler. T., Van Bruggen. M.P.B., Apetz. R (2003) "Transparent sintered corundum with high hardness and strength" Journal American Ceramic Society **86**, 12–18.

Wang. C., Ping.W., Bai. ., Cui. H., Hensleigh. R., Wang. R., Brozena.A.H. Xu. Z., Dai. J., Pei. Y., Zheng. C., Pastel. G., Gao. J., Wang.X., Wang. H., Zhao. J.C., Yang. B., Zheng. X., Luo. J., Mo. Y., Dunn. B., Hu. L (2020) "A general method to synthesize and sinter bulk ceramics in seconds, Science **368**, 521-522.

Yu. M., Grasso. S., Mckinnon. R., Sunders. T., Reece. M. J (2017) "Review of flash sintering:materils, mechanisms and modeling," Advanced Applied Ceramics **116,** 24-60,

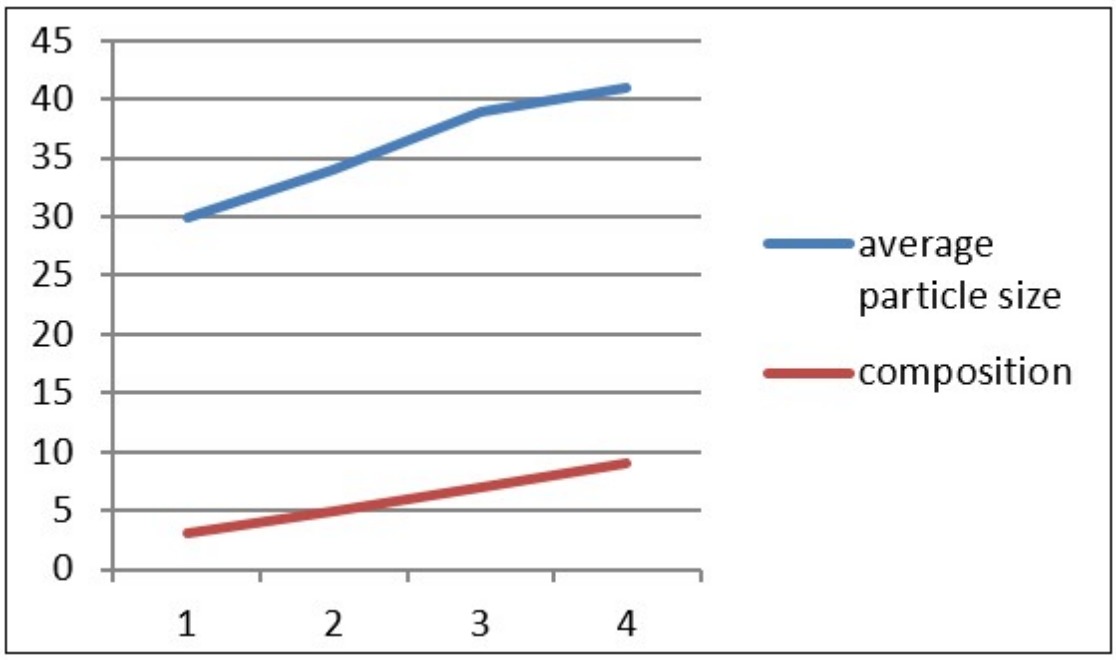

Figure 1: Average particle size versus alumina nanoprecursor composition

Table 1: Prerequisites and parameters of cold compaction.

Composition	Pre-calcination at temp/time (ºC/hour)	Binder (2%)	Pressure (MPa)	Time (seconds)
A1, A2, A3 & A4	400/1	PVA	100	3

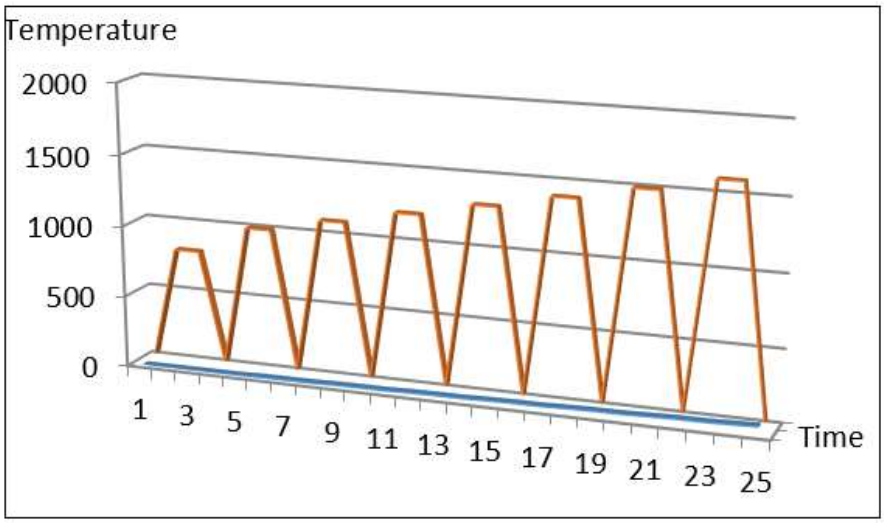

Figure 2: Heating programme –I

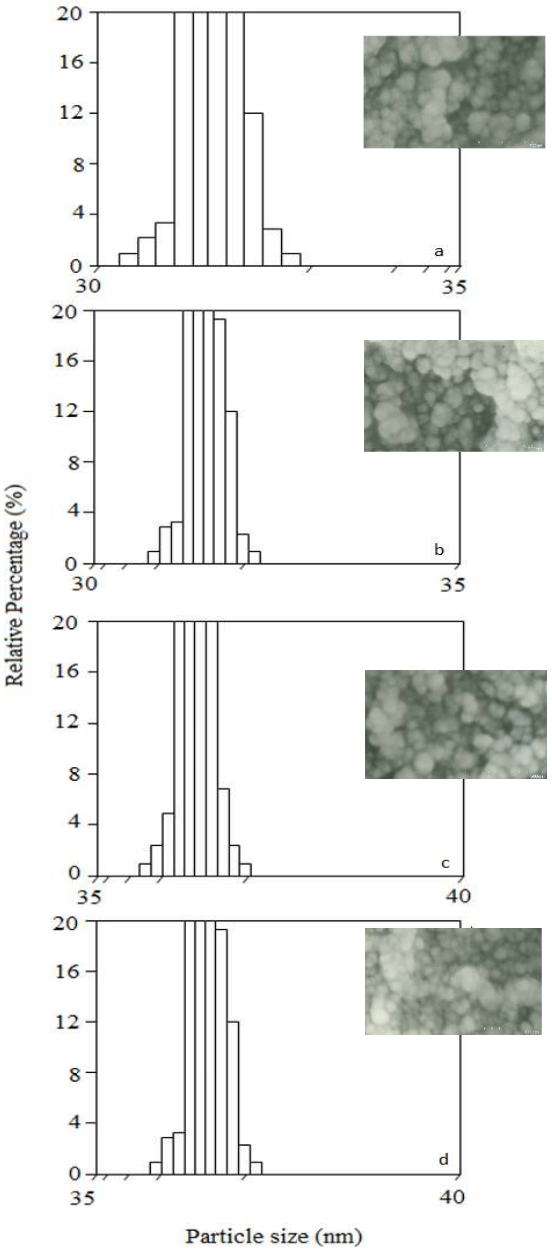

Figure 3: Particle size distribution of q) A1, b) A2, c) A3 and

d) A4 alumina powders with respective SEM micrograph

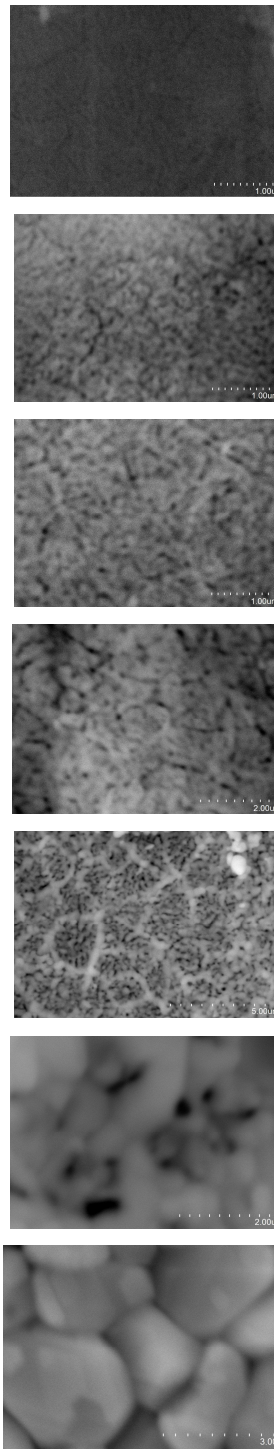

Figure 4: a). A1 after firing at 1000º, b) after firing at 1100ºC, c) after firing at 1200ºC, d) after firing at 1300ºC, e) after firing at 1400ºC, f) after firing at 1500ºC, g) after firing at 1600ºC.

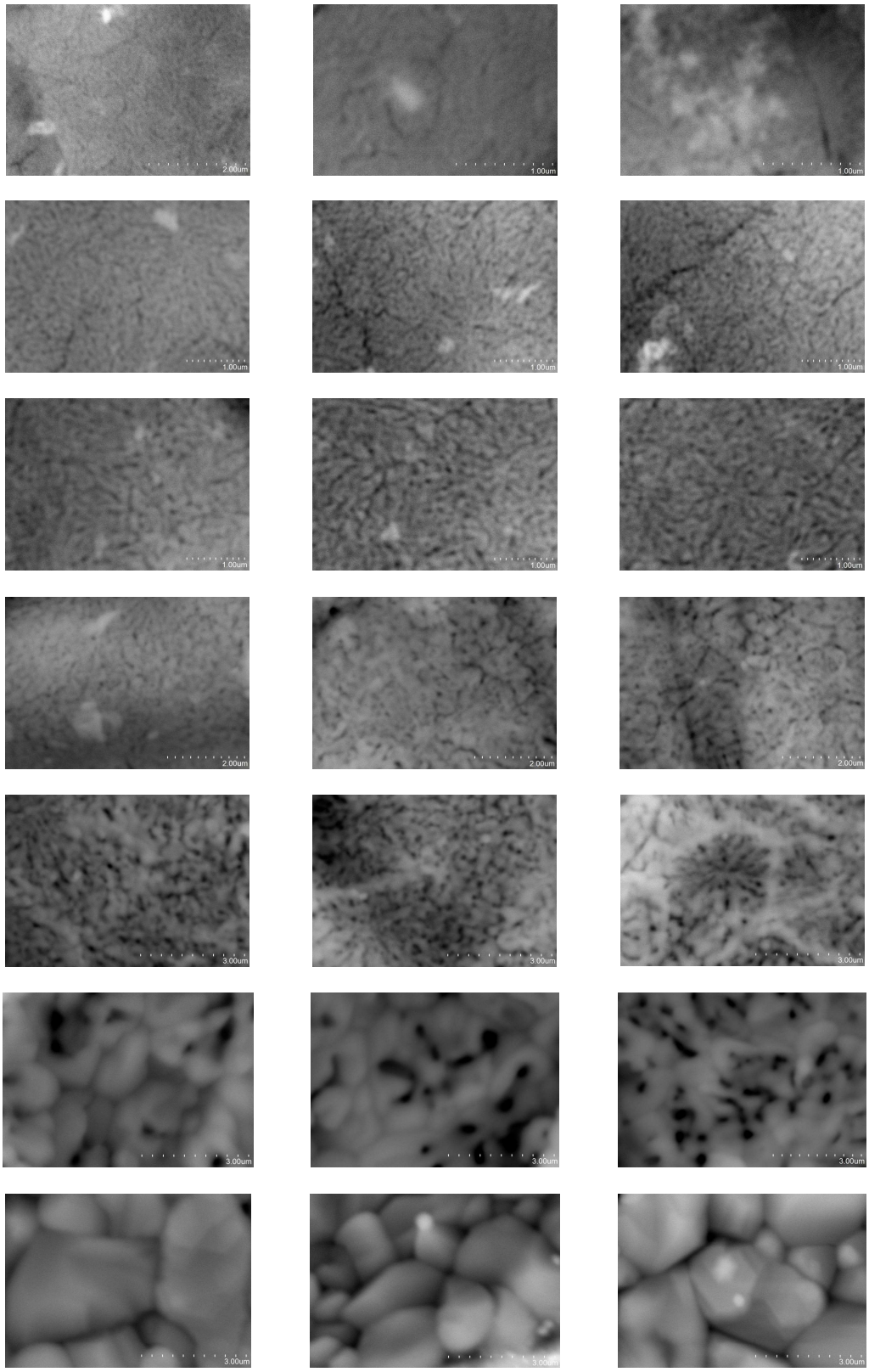

Figure 5: A2, A3, A4 compositions after firing at 1000ºC, 1100ºC, 1200ºC, 1300ºC, 1400ºC, 1500ºC and 1600ºC (Heating schedule-I).

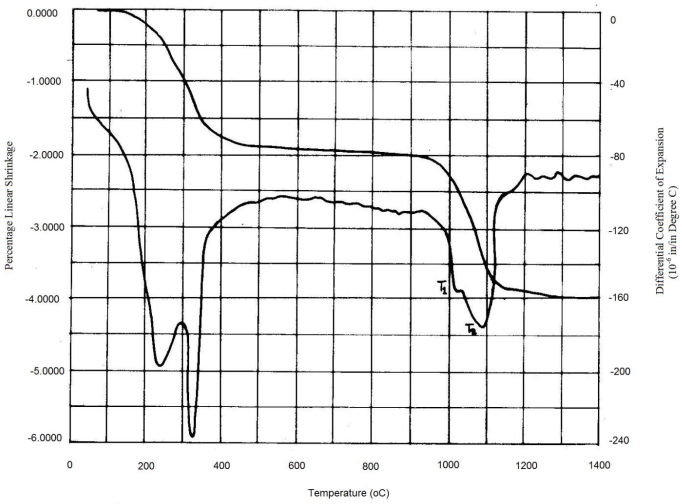

Figure 6: : Dilatometric curve of A1 composition.

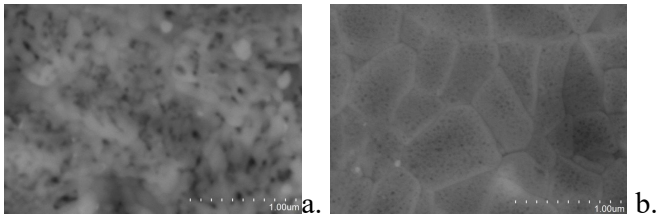

Figure 7: A1 composition after firing at a). 1000°C and b). 1400°C (Heating schedule-II).

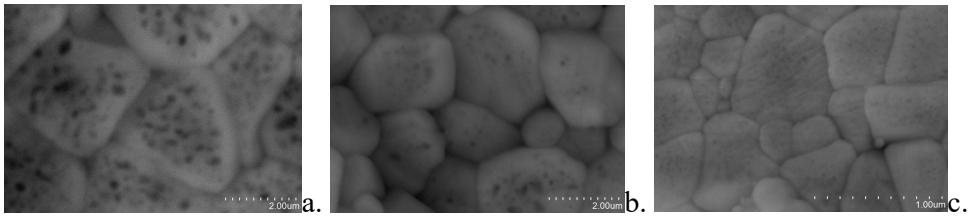

Figure 8: a) A2, b) A3, c) A4 after firing at 1400°C (Heating schedule-II).

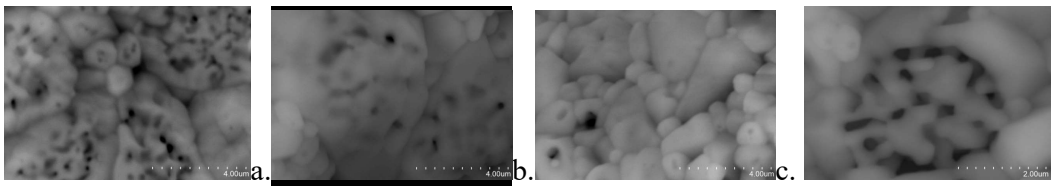

Figure 9: Mechanism of bimodal grain growth during heating schedule-I.

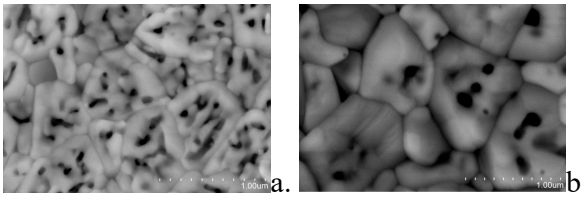

Figure 10: Frame work of pore population and grain growth during heating schedule-II.